Detecting Grasp Phases and Adaption of Object-Hand Interaction Forces of a Soft Humanoid Hand Based on Tactile Feedback

Pascal Weiner, Felix Hundhausen, Raphael Grimm and Tamim Asfour

***Abstract*— Engineering humanoid robot hands with the ability to dexterously grasp objects of different sizes, shapes, material properties and weights requires sophisticated tactile sensing and intelligent controllers able to interpret sensory information and adapt contact forces with the object to achieve a stable and safe grasp. In this paper, we present a new soft humanoid hand equipped with a multimodal sensor system in each finger and a human-inspired grasp-phases controller that is able to detect the different phases of a grasping and manipulation task, adapt interaction forces with the manipulated object and balance the force distribution in both precision and power grasps based on tactile feedback. To evaluate the controller, we conducted experiments with the hand on the humanoid robot ARMAR-6 and 31 different soft and rigid everyday objects and food items with weights ranging from $4.8\,\mathrm{g}$ of a paper cup to $1133.8\,\mathrm{g}$ of a bottle, different shapes and material properties. The results show that grasping force can be reduced by 65% compared to a naive grasping approach using maximum force for grasping and manipulating both fragile objects without destruction as well as heavy objects.**

I. Introduction and Related Work

Robust grasping of unknown objects with varying shape, weight, stiffness, fragility, material properties and changing center of mass remains a challenging problem [1], yet fundamental to truly endow both humanoid robots and prostheses with the abilities needed to perform dextrous grasping and manipulation tasks. Engineering such capable hands requires not only the integration of mechanics including actuators, sensors and embedded systems in limited space, but also the development of intelligent controllers able to interpret multimodal sensory data and to adapt to different objects and tasks. A key requirement on such controllers is the ability to continuously estimate and update grasping forces applied on an object to ensure safety and stability of the grasp.

To implement such force adaptation strategies, tactile feedback at the contact points between hand and object is crucial to describe their interactions in the different phases of a grasp, i.e. to detect initial contact and adapt the applied forces to establish a stable grasp, to lift, hold and replace the object. An overview on the use of tactile information in grasping and manipulation tasks is presented in [2]. In this work, we present a novel soft humanoid hand, see Figure 1, which is equipped with a multimodal sensor system and

This work has been supported by the German Federal Ministry of Education and Research (BMBF) under the project INOPRO (16SV7665), the Helmholtz AI project LearnGraspPhases, the KIT Centers pilot project SoftNeuro and the JuBot project founded by the Carl Zeiss Foundation.

The authors are with the Institute for Anthropomatics and Robotics, Karlsruhe Institute of Technology, Karlsruhe, Germany {pascal.weiner, asfour}@kit.edu

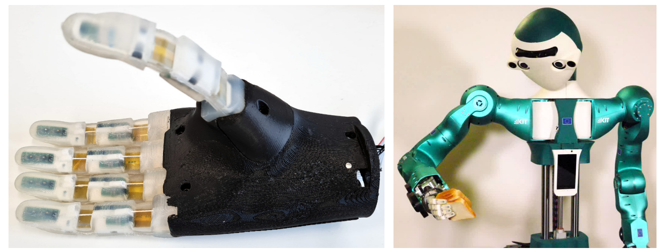

Fig. 1: Soft humanoid hand with multimodal sensor system attached to the humanoid robot ARMAR-6

controllers for the adaption of object-hand interaction forces in the different phases of grasping and manipulation tasks.

Numerous control strategies for grasping unknown objects introduced in the literature share the common goal of estimating and controlling the friction coefficient at contact points between the hand and the object. This is either achieved through measurement of shear and normal forces [3]–[5], slip detection and prevention [6]–[11], or a combination of both [12]–[14]. In [4], the control target is explicitly formulated in terms of the friction coefficient based on normal and shear forces estimated from raw sensor data using machine learning. A similar formulation has been used in [5] on the basis of 3D-force sensors. The authors in [12] use a optoelectronic sensor array and machine learning for determining normal and shear forces for friction coefficient based control. Thereby, objects are explored to estimate the friction coefficient and the noise in the shear force signal is used for slip detection. The work has been extended in [13] to allow an online estimation of the friction coefficient. A similar approach for the online estimation of the friction coefficient at each contact point for the manipulation of heavy deformable objects based on optoforce sensors data is described in [14].

A different approach is to explicitly deal with the problem of slip detection. In [15], a hybrid position/force controller is employed for grasping where the controller target values are adapted based on slip signals. Slip detection and grasp force adaption based on normal, shear and torques measured at the contact points was shown in [7]. A similar system is implemented using a velocity-based force controller in [8] that increases the applied force at the contact points once slip is detected. The authors in [9] present a rule-based system for grasping utilizing slip detection. A human-inspired grasp stabilization controller based on tactile feedback is presented in [10], where each finger is independently controlled based on slip detection and a leaky integrator-based velocity controller. This distributed control approach ensures stability of a grasp in complex in-hand-manipulation tasks. In [11], a neuromorphic controller is used where slip events are encoded by spikes and used as input for a monotonic PI controller.

Other works deal with the estimation of the required normal force based on object stiffness/material. In [16], the stiffness is estimated based on the distance change between the gripper yaws during initial contact. A similar approach is used in [17] and [18] and extended to detect slip in grasping with prosthetic hands and a gripper. In [19], an online method for simultaneous detection of contact events and object material based on tactile data is presented.

Few works approach the problem of developing grasping controllers that adapt grasping forces during the different phases of a grasp and manipulation task. In [20] four different behaviors for gentle closing, holding, handover and in-hand manipulation are implemented using feedback from a vision-based tactile sensor. Research about sensorimotor control in humans [21] reveals that grasping and manipulation tasks consist of a sequence of the action phases *reach, load, lift, hold, replace* and *unload*. These phases are defined and characterized by contact events and force profiles at the contact points to allow a smooth transition between consecutive phases of such tasks. Inspired by [21], the authors in [16] describe a grasp controller for picking up and placing an object based on tactile events derived from pressure arrays attached to the yaws of a parallel gripper and a accelerometer. The work shows how tactile feedback can be used to complete a grasping and manipulation task on a robot. Our work shares similarities with this work as we use the same strategy regarding the decomposition of a grasping and manipulation task in different phases. However our work extends the approach to soft humanoid robot hands including synchronization between actuators.

Recently, soft anthropomorphic hand designs and their sensorization have been studied to increase robustness and safety of grasping while exploiting natural interaction with the objects and passive compliance and/or active regulation of grasping forces [7], [22]–[27].

In this work, we present a novel version of a soft humanoid hand by combining our previous development of soft fingers [28] and sensorized fingers [29]. The new soft fingers are equipped with normal force sensors, 3D-shear force sensors, proximity sensors and accelerometers. The fingers are attached to an under-actuation mechanism to control all fingers with only three motors. Using this new hand, we develop a human-inspired grasp-phases controller that is able to detect the different phases of a grasping and manipulation task, adapt interaction forces with the manipulated object and balance the force distribution in both precision and power grasps based on tactile feedback. In contrast to most works in the literature, we do not restrict the grasps such that contact points are located on sensorized surfaces, but explicitly deal with incomplete sensory information. We evaluate the controller on a humanoid robot in grasping and manipulation experiments with 31 objects of different sizes, shapes, material properties and weights.

(a)

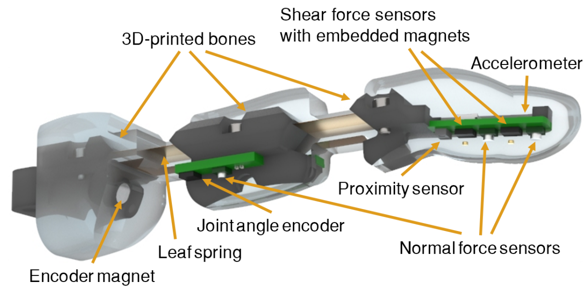

(b)

Fig. 2: (a) Palmar side of the soft finger. (b) Section view through the fingers silicone and distal bone exposing the internal structure and sensors visible from this side. The PCB with sensors on the intermediate phalanx covers both sides of the finger, as can be seen in (a).

II. The KIT Soft Humanoid Hand

The soft humanoid hand combines our previous developments of soft fingers [28] and sensorized fingers [29]. The hand is driven by three DC motors, where thumb and index finger are actuated independent by one motor each and the remaining fingers are actuated by the third motor via an underactuation mechanism. Here, we provide a description of the hand, in particular the soft fingers and their sensor system, as well as a brief description of the hand mechanics.

A. Soft Finger Design

The mechanical design of the soft fingers is based on our previous work [28]. These fingers are comprised of 3D-printed bones for the distal, intermediate and proximal phalanx, connected by a leaf spring. The bones are encased in soft silicone and actuated using a tendon. Compared to the fingers in [28], in which each finger tip is equipped with a high resolution camera, we have adapted the mechanical structure of the finger to printed circuit boards (PCBs) mounted on the distal and intermediate bones of the finger. The plastic leaf spring in the original design has been replaced by a steel leaf spring with 90 µm thickness, which also made it possible to attach the spring to the bones using screws instead of glue. Two flat flex cables are taped to the spring, connecting the PCBs at the finger bones. An overview of the design of the fingers is depicted in Figure 2.

B. Embedded Sensor System

The sensor system used in the fingers is based on work presented in [29] originally developed in a setting with rigid fingers. The work includes an in-depth characterization of the sensor system and its different modalities. The sensor system includes normal and 3D-shear force sensors, accelerometers, joint angle encoders and proximity sensing in each finger. Our approach toward the realization of sensorized humanoid hands relies on using commercially available off-the-shelf components and fabrication techniques to allow a reproduceable design. Hence, we use digital sensors on standard PCBs, which are connected to a central processing unit by a digital bus (I^2C). We notably include barometer-based normal force sensors as well as Hall effect-based 3D-shear force sensors which can both measure forces in normal direction. The barometer-based sensors are more sensitive and are used to augment the readings of the 3D-shear force sensors, as explained in Section III. For the design of the sensor system for the soft hand in this work, we adapted all but two sensing modalities. Unchanged are the accelerometers in the fingertip as well as the 3D-shear force sensors.

We replaced the time-of-flight based distance sensor by a proximity sensor since the silicone reflects some light and hence interferes with the time-of-flight measurement. Inspired by the results presented in [30], we integrated an infrared proximity sensor (VCNL4040, Vishay Semiconductors) at the base of the distal phalanx. Since the soft fingers have no clear axis of rotation in the joints and can also additionally twist, the joint angle measurement has also been adapted. We placed a magnet at the distal and proximal phalanx facing the respective joint and two 3D hall effect sensors at the intermediate phalanx facing these magnets. If the joint is actuated, the magnet moves closer to the sensor. This results in a nonlinear but monotonic signal that has been measured and fitted using a piecewise linear function.

Lastly, we adapted the barometer-based sensitive normal force sensors. The design we presented in [29] uses barometers with a metal lid and a miniature hole for air, which made it necessary to encase them with small casted silicone covers. The cover ensured that an air pocket is formed above the sensor, transducing the pressure through the miniature hole in the lid to the sensor. Another work circumvented the problem by carefully removing the lid, drilling the hole open and glueing the lid back onto the sensor [31]. For the soft fingers we now use barometers usually used for medical applications (LPS27HHW, ST Microelectronics), which feature an exposed sensor covered by soft gel. It is hence possible to directly cast the sensors into silicone without any prior modifications or additional covers, which greatly eases production. The barometer-based normal force sensors show a similar performance to the ones described in our previous work.

C. Underactuated Hand with Embedded System

Five of the soft fingers described above are used for the realization of an underactuaded anthropomorphic hand. The design is based on our previous design presented in [28] and described here briefly for completeness. The hand includes three identical DC gear motors, where thumb and index fingers are driven by one motor each and the remaining fingers are driven by the third motor via and an underactuated mechanism. This mechanism allows each of the three fingers to close even if others are blocked, hence the fingers can wrap around the object to conform to the object's shape. Through a block and tackle system, the force on the motor tendon is tripled and distributed adaptively to the three fingers at the cost of three times the closing time. Hence, the force acting on little, ring and middle finger is roughly the same as the force acting on the individually actuated index finger and thumb since all motors are identical. This greatly eases the development of force control algorithms, as all fingers behave the same apart from closing speed. The completed hand with sensorized fingers is shown in Figure 1.

The hybrid embedded system for sensor data processing and control consisting of a microcontroller and FPGA integrated in the palm is the same as in [28]. In this work, we use the FPGA to read the ten buses to all sensor PCBs in the fingers in parallel with a sample rate of 140 to $160\,\mathrm{Hz}$ depending on processor timings. Multiple accelerometer values are transmitted in each frame since the accelerometer samples at $1.6\,\mathrm{kHz}$. The aggregated sensor data is then passed to the microcontroller and from there to the EtherCAT bus of the humanoid robot ARMAR-6 we use in our experiments.

III. Grasp-Phases Controller

Our goal is to realize a human-inspired grasping controller that is able to (i) detect the different phases of a grasping and manipulation task, (ii) adapt interaction forces with the manipulated object and (iii) balance the force distribution in both precision and power grasps based on tactile feedback provided by the multimodal sensor system of the soft humanoid hand. This grasp-phases controller should be able to stabilize unknown objects during the whole grasping process, while minimizing the force exerted on the object based on tactile feedback. The code of the controller is publicly available[1]. To integrate with the EtherCAT bus used on our humanoid robot ARMAR-6, the controller has to run with at least $1\,\mathrm{kHz}$. Using this grasp-phases controller, the hand should be able to grasp and lift fragile objects like a plastic cup or toast without crushing it, while stabilizing heavy objects such as water bottles. Inspired by sensorimotor control in human grasping and manipulation [21], we consider all phases of a grasping and manipulation task, i.e., closing the fingers to establish contact with the object, lifting, holding, manipulating and placing the object.

The proposed grasp-phases controller is designed to grasp and manipulate unknown objects, without prior knowledge about object size, weight or shape. Hence, the controller has to infer the necessary grasping force purely based on sensor information at run-time and adapt forces at contact points in a reactive way. Figure 3 depicts the structure of the grasp-phases controller and employed control laws.

Each of the three motors is controlled separately by its own motor controller based on sensors in the fingers associated with the motor: The thumb motor is controlled based on sensors inside the thumb, the index motor based on sensors in the index finger and the third motor based on signals from the remaining three fingers. It has been shown that such

[1]Code available Online at: `https://gitlab.com/ArmarX/Armar6RT/-/blob/master/source/Armar6RT/libraries/KITSensorizedSoftFingerHandV1NJointControllers/MinimalGraspingForceV1.h`

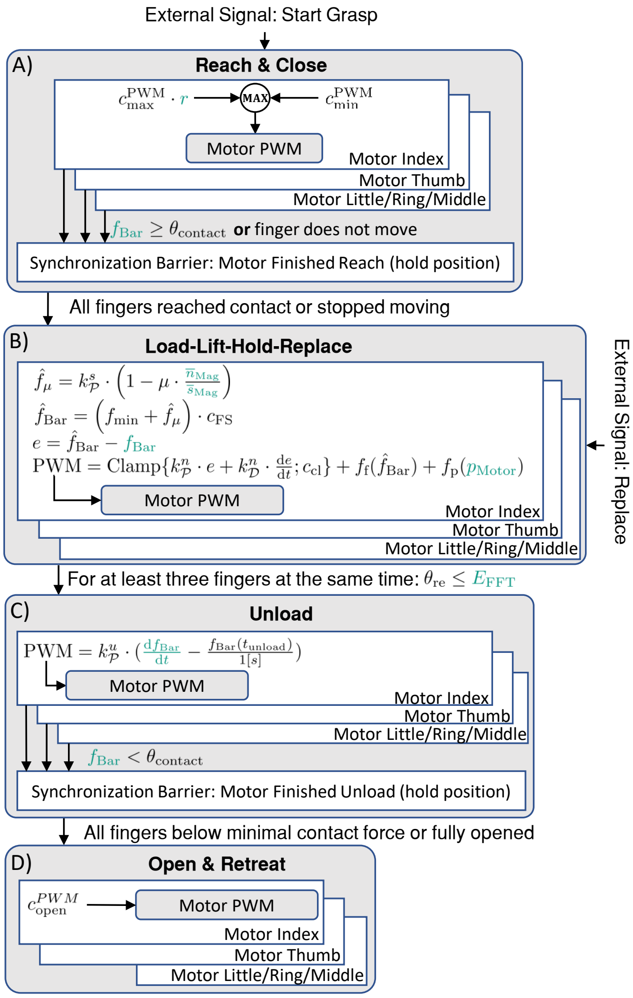

Fig. 3: State machine of the proposed grasp-phases controller. Values in green are values continuously calculated based on the the hand sensor signals

an approach can reduce control complexity while ensuring the overall grasp stability based on the interaction between decentralized controllers through the object [10]. In this work, the three motor controllers are synchronized at the end of each grasp phase so that they start the new phase only if all fingers are ready.

The design of the grasp-phases controller follows two main principles: a) taking inspiration from human grasping and b) minimizing the number of necessary control parameters.

a) Human-inspired Phases of grasping and manipulation tasks: The soft humanoid hand with its human-like shape and sensing modalities is predestined for the implementation of a human-inspired approach to grasping. Therefore, we divided the grasp-phases controller following the concept presented in [21] into the four grasping phases *reach & close*, *load-lift-hold-replace*, *unload* and *open & retreat*. Transitions between these phases are defined by contact events or sudden changes in interaction forces. Compared to the grasping phases in [21], our grasp-phases controller maps the four grasping phases load, lift, hold and replace to one single phase (*load-lift-hold-replace*). We consider this assumption reasonable as, except the load phase, the lift, hold and replace phases are mainly concerned with arm motion and share similar goals in terms of object stabilization and force control. The goal of the grasp-phases controller, with its four sub-controllers for the four phases, is to robustly grasp objects with different properties such as size, weight and shape while ensuring the right amount of force to avoid squashing the object in the hand.

The grasp-phases controller generates pulse width modulation (PWM) targets for each motor based on only two external control signals: (i) The command to start object grasping and (ii) a signal indicating that the object will soon be replaced. As the controller does not rely on additional external information, it is also easy to use in the context of prosthetic hands, where only information from sensors embedded into the hand is available.

b) Design of the sub-controllers: For the sub-controllers, the number of control parameters can drastically influence the amount of time needed to tune the controller. Hence, we aim – wherever possible – to reduce the number of engineered control parameters. Furthermore, we selected parameters that are intuitively explainable, either in the context of the human grasping process or based on physical laws. Due to sensor offsets in the measurement of normal and shear force that depend on several changing conditions such as room temperature and atmospheric pressure, the controller automatically determines such offsets by continuously averaging these sensor values when the controller is inactive.

In the following we describe the different grasp phases and the implementation of their sub-controllers.

A. Reach & Close Sub-Controller

In this work, we assume a pre-defined grasping pose for the hand, as finding a suitable grasping pose for unknown objects goes beyond the scope of this work. The grasp-phases controller is started by an external signal which starts the *reach & close* sub-controller for each motor. As the grasp should be executed as fast as possible, the fingers initially close with the maximum PWM $c_{\max}^{\mathrm{PWM}}$. To avoid hitting the object at maximum speed, the finger velocity is then scaled based on the sensor data of the proximity sensor. The values r of proximity sensor are normalized to the interval $[0,1]$ where 1 indicates that no object is in the range of the sensor, i.e., no reflected light is detected, and 0 indicates that the the finger has contact with the object, i.e., a maximum amount of light is reflected. The proximity signal of the sensor depends on the reflectance of the object. Nonetheless, the signal has proven suitable for a large range of objects. Hence, the maximum PWM is scaled by the proximity sensor data $r \cdot c_{\max}^{\mathrm{PWM}}$ to reduce the speed and gently establish contact with the object (see Fig. 3-A). Due to this normalization, the fingers proportionally slow down as they reach a distance of around 2 to $3\,\mathrm{cm}$. To make sure that the fingers establish contact with the object, the maximum value of $r \cdot c_{\max}^{\mathrm{PWM}}$ and $c_{\min}^{\mathrm{PWM}}$ is used, where $c_{\min}^{\mathrm{PWM}}$ is the minimum PWM required to slowly close the fingers. Such slow closing of the fingers is also important to prevent damage of the object.

Contact with the object is detected by the contact threshold $\theta_{\mathrm{contact}} \leq f_{\mathrm{Bar}}$ on the maximum signal f_{Bar} from the sensitive barometer based normal force sensors. Specifically, the maximum is taken over the barometers placed at the left and right of the proximal phalanx (B_{ProxL}, B_{ProxR}), at the distal phalanx next to the joint (B_{DistJ}) and next to the tip (B_{DistT}), as shown in Equation 1.

$$f_{\text{Bar}} = \max\{B_{\text{ProxL}},\ B_{\text{ProxR}},\ B_{\text{DistJ}},\ B_{\text{DistT}}\} \tag{1}$$

For the motor actuating little, ring and middle finger, the maximum over all three fingers is taken. As soon as any finger sensor detects contact, the motor switches to position control mode to hold the position at which the contact occurred. When grasping an object with protruding edges, the finger may make contact with the object that is not detected by any normal force sensor because the sensors do not cover the entire finger. As a fallback for this case, we use the relative motor encoder to detect if the finger has stopped moving. This also covers the case where the finger misses the object and closes completely. The contact position is then held until the other two motors also bring their fingers into contact with the object or close the corresponding finger(s) completely. When all three motors are either in hold position mode or stopped moving, the sub-controllers of all three motors trigger the next phase. As described in [32], this contact sensing based closing behavior has advantages compared to closing the hand without sensor feedback, even in the presence of adaptive underactuation and passive compliance.

B. Load-Lift-Hold-Replace Sub-Controller

As soon as all fingers have detected contact with the object or have stopped moving, the motor controllers switch to force control mode for each motor and directly output PWM targets. Each motor acts based on the maximum over all barometer-based normal force sensor values f_{Bar} measured in the fingers actuated by the motor.

The force controller consists of two feedforward terms as well as a PD-controller. The first feedforward term $f_{\text{p}}(\cdot)$ takes the relative motor encoder position p_{Motor} and calculates the PWM necessary to hold it. This term hence cancels the progressive spring forceand is realized as piece-wise linear function obtained by slowly increasing the PWM of the motor and recording the relative motor encoder position p_{Motor}. The second feedforward term $f_{\text{f}}(\cdot)$ takes the target force $\hat{f}_{\text{Bar}}$ as input and outputs a PWM value that produces this target. The piece-wise linear function representing this term was obtained by letting the index finger in a fully opened state press against a flat surface with increasing PWM while recording f_{Bar}. Lastly, a PD-controller reduces the error of the feedforward terms. This term is clamped to a value of $\pm c_{\text{cl}}$, so that, if none of the barometers is in contact with the object, the controller outputs reasonable values based on the feedforward terms. The force is controlled based on the barometer based force sensors since these are far more sensitive compared to the Hall effect sensors. The force controller can be expressed by Equation 2 (see Fig. 3-B):

$$\begin{aligned} e &= \hat{f}_{\text{Bar}} - f_{\text{Bar}} \\ \text{PWM} &= \text{Clamp}\{k^n_{\mathcal{P}} \cdot e + k^n_{\mathcal{D}} \cdot \frac{\mathrm{d}e}{\mathrm{d}t}; c_{\text{cl}}\} \\ &\quad + f_{\text{f}}(\hat{f}_{\text{Bar}}) + f_{\text{p}}(p_{\text{Motor}}) \end{aligned} \tag{2}$$

The normal force target $\hat{f}_{\text{Bar}}$ is calculated by a P-controller acting on the normal to shear force ratio (Equation 3), with an offset defined by a fixed term of $f_{\min}$ (Equation 4). The fixed term ensures that the force controller always retains a small contact force with the object. For the overlying friction control, we assume a fixed friction coefficient μ. The shear and normal forces $\overline{s}_{\text{Mag}}$ and $\overline{n}_{\text{Mag}}$ are calculated over all fingers as an average over all *active* shear force sensors. A sensor is deemed *active* if the barometer between these two sensors indicates contact. We explicitly use the normal force component of the Hall effect sensors instead of the barometer values for this calculation so that all measurements share the same measurement principle. For the sake of simplicity, we assume here that the surface normal of the object coincides with the normal force direction of the shear force sensors. The shear force controller is implemented as follows:

$$\hat{f}_{\mu} = k^s_{\mathcal{P}} \cdot \left(1 - \mu \cdot \frac{\overline{n}_{\text{Mag}}}{\overline{s}_{\text{Mag}}}\right) \tag{3}$$

$$\hat{f}_{\text{Bar}} = \left(f_{\min} + \hat{f}_{\mu}\right) \cdot c_{\text{FS}} \tag{4}$$

The target forces are scaled by the factor c_{FS} (Equation 5), for all fingers other than the thumb so the four opposing fingers do not force the thumb open.

$$c_{\text{FS}} = \begin{cases} 1 & \text{if thumb} \\ \frac{1}{3} & \text{else.} \end{cases} \tag{5}$$

We used the factor $\frac{1}{3}$ instead of $\frac{1}{4}$ for balancing the four fingers opposing the thumb to compensate for friction in the mechanism and rope guides.

C. Unload and Open & Retract Sub-Controllers

The *unload* sub-controller is triggered by an external signal from the robot control PC, indicating the intent to soon place the grasped object. This prevents triggering object unloading in the case of accidental contact events with the environment while performing a transfer motion. Once the external signal is received and contact with a supporting surface is detected, the controller starts to reduce the forces applied to the object to replace it in a controlled manner. Contact is detected if at least three of the accelerometers embedded in each finger tip sense vibrations in the range of 400 to $800\,\text{Hz}$ of the fast Fourier transform of the accelerator signals in a window with the last 32 measurements and a total energy over θ_{re}. This indicates the start of the unloading phase. For each motor, the rate of change in pressure $\frac{\mathrm{d}f_{\text{Bar}}}{\mathrm{d}t}$ is controlled by a P-controller with $k^u_{\mathcal{P}}$, setting a PWM target (see Fig. 3-C). The target rate of change is calculated at the beginning of the phase such that unloading of the object is expected to finish within one second. As soon as all fingers driven by the motor

TABLE I: Controller parameters.

Parameter	Value	Parameter	Value	Parameter	Value
$c_{\max}^{\mathrm{PWM}}$	100%	$c_{\min}^{\mathrm{PWM}}$	30%	θ_{re}	40000
$\theta_{\mathrm{contact}}$	21 mbar	c_{cl}	11%	$k_{\mathcal{P}}^{s}$	5000
$k_{\mathcal{P}}^{n}$	1	$k_{\mathcal{D}}^{n}$	0.2	$k_{\mathcal{P}}^{u}$	-15
$f_{\min}$	120 mbar	μ	0.4		

reach a value below a contact threshold $f_{\mathrm{Bar}} < \theta_{\mathrm{contact}}$, the motor switches to position control mode and holds the current position until all motors finished unloading, i.e., all fingers are no longer in contact with the object.

The *unload* phase is considered completed when all fingers have either lost contact with the object or are completely opened. In the subsequent *Retreat* phase, see Fig. 3-D, the fingers open with maximum motor speed to the maximum hand aperture.

IV. Experimental Evaluation

The grasp-phases controller is evaluated experimentally by grasping everyday objects and food items using the humanoid robot ARMAR-6 [33] and compared against the baseline approach of grasping with maximum force. The parameters used in all evaluation experiments are listed in Table I. The control parameters strongly depend on the used hardware and sensors. Hence, they have been experimentally chosen based on a test set of objects that is completely disjoint from the set used in the evaluation. Only subsets of parameters have to be tuned at the same time as they are partitioned into the different phases, such as $\{k_{\mathcal{P}}^{s}, \mu, f_{\min}, k_{\mathcal{D}}^{n}, k_{\mathcal{P}}^{n}, c_{\mathrm{cl}}, \theta_{\mathrm{re}}\}$ or $\{k_{\mathcal{P}}^{u}, \theta_{\mathrm{contact}}\}$. The chosen value for μ has proven to be a good estimate of the friction acting between the silicone fingers and textureless surfaces. In our experiments, we use 31 different objects, see Figure 4. The objects include three drinking vessels that are grasped with two different liquid levels, resulting in 31 grasps of objects with different properties. Object weight varies from $4.8\,\mathrm{g}$ for the paper cup to $1133.8\,\mathrm{g}$ for the plastic cola bottle. For the heavy objects, different materials are chosen (metal, plastic, glass) to assess the performance of grasping and lifting objects with different friction coefficients. The object set also contains rigid and soft objects like the elephant plushie, the capri sun bag and the sponge. The execution on the robot is completely decoupled from the grasp-phases controller since the controller only receives two commands from the robot in each grasping trial: the command to trigger grasping and the signal indicating that the object will soon be replaced.

A. Experiment Protocol

The experiments are carried out with the hand attached to the right arm of the robot, see Fig. 1. Each object is placed on the table at a pre-defined position. Each grasp trail is carried as follows: (1) We use kinesthetic teaching to guide the robot arm in zero-torque mode to a pre-grasp and grasp pose. We explicitly consider the reaching motion through pre-grasp and grasp pose as we are in general interested in the whole grasping and manipulation task. The grasp pose is chosen so that the grasp is aligned with the longest object axis. (2) Start the experiment with the arm in fixed starting position. (3) The

Fig. 4: Set of objects used in the experiments. From left to right and back to front: chips, rectangular empty bottle, cola glass, PET bottle, cola plastic, sponge, metal bottle, mustard bottle, potato starch, empty capri sun, empty can 333ml, empty can 500ml, full boxed juice, elephant plushie, full capri sun, boxed juice empty, peppermint tea, salt sticks apple, bell pepper, papercraft box, paper cup, plastic cup, orange, toast slices, jelly cup, yeast dumpling, ice cone, bananas, mie noodles

arm moves to the pre-defined pre-grasp and grasp pose and triggers the *reach & close* phase sub-controller. (4) As soon as the controller has reached the load phase, the object is lifted and moved to the right of the table. (5) The hand is rotated approximately $45°$ using wrist pronation/supination and flexion/extension to disturb the grasp. (6) The arm moves the object back to the pre-defined grasping position on the table and informs the grasp-phases controller that the object can now be replaced. (7) The hand moves down until the grasp-phases controller enters the unload phase. (8) The arm moves back to the fixed initial position. For the baseline approach, the same protocol is used with the difference that the object is grasped with maximum force and lifted after a $3\,\mathrm{s}$ delay. Further, the object placement is realized by detecting contact with the table using the 6D-force/torque sensor in the wrist of the arm. The execution of these grasping trials is shown in the accompanying video. Example grasps are depicted in Figure 5. Depending on the object height, a top or side grasp was taught. Top grasps were for example chosen for the bananas, the tea, yeast dumpling and apple.

B. Results and Discussion

For the evaluation, we consider several aspects that are important to assess the quality of grasps in the conducted experiments: a) The generated grasping force, b) the number of dropped objects and c) the number of damaged objects.

a) Grasping Force: The amount of grasping force is quantified in terms of motor effort, i. e. the time of PWM modulation in percent. The baseline approach always utilizes $100\,\%$ motor effort. For the grasp-phases controller, this value is calculated by taking the average of the motor PWM at each time step during the execution, beginning with the closing of the fingers in the reach phase and ending at the end of the *open & retreat* phase. Since each motor receives different targets, the values are calculated for each individual motor. Over all motors and grasping trials, the average motor effort is $35.64\,\%$. The results for each motor and each grasping trial

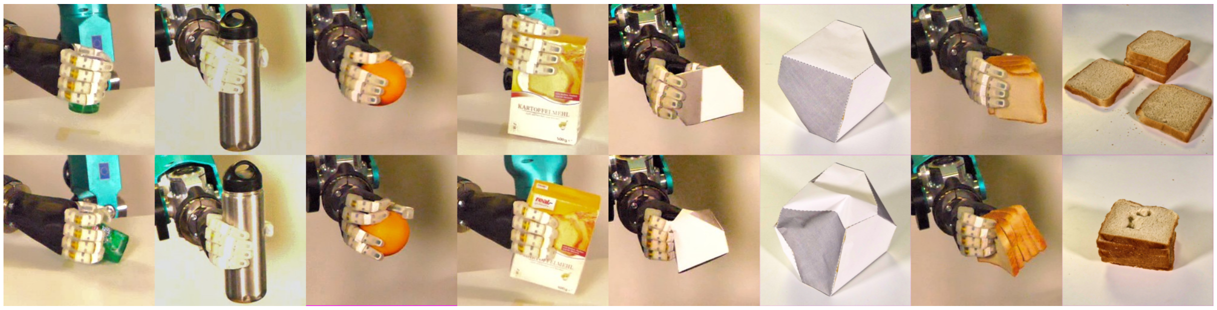

Fig. 5: Example grasps using our approach (top row images) and the baseline approach (bottom row images).

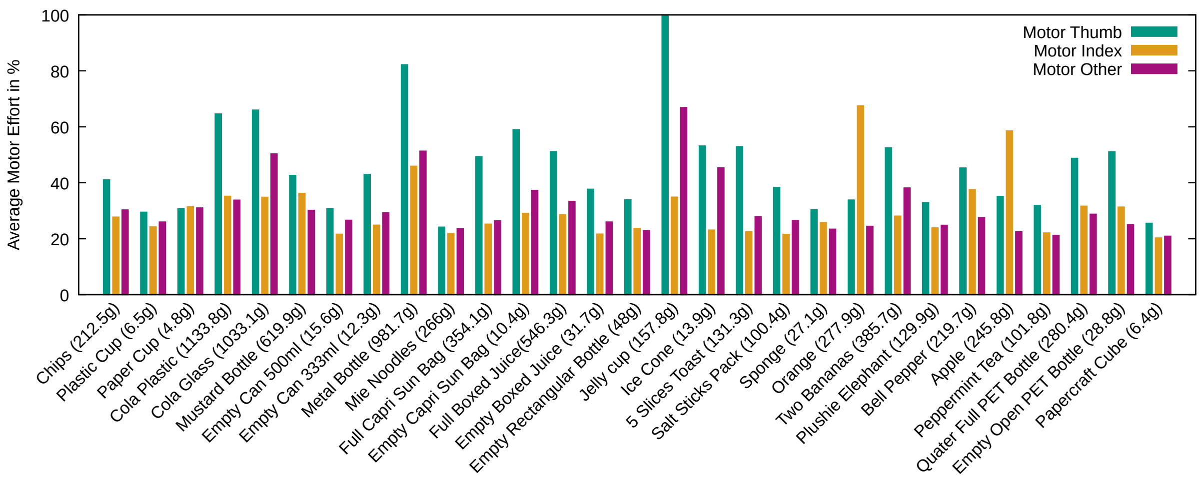

Fig. 6: Motor effort averages calculated over the duration of the experiments for the grasp-phases controller. While the baseline always requires $100\,\%$, the grasp-phases controller uses averaged over all objects only $35.64\,\%$. As a result, the grasp-phase controller transmits less force to the object and thus avoids damaging fragile objects.

are shown in Fig. 6. Evidently, the controller generates higher motor efforts for heavy objects without a form closure grasp as in the case of the metal bottle and the boxed juice. The controller also generates higher targets for deformable objects like the empty capri sun bag, the pet bottle and the toast. This is caused by high perceived shear forces, which are most likely induced by the fingers deforming the object, causing the fingers to drag along the surface. The jelly cup shows a clear anomaly, caused by its geometry. While grasping the cup, contact occurred at the protruding edge at the top of the cup where the lid is glued to, resulting in excessive shear forces and low normal forces, probably since the silicone of the finger was distorted locally due to the sharp edge.

b) Dropped Objects: The baseline approach was able to lift and hold all objects except the jelly cup in all experiments while the grasp-phases controller was not able to lift the yeast dumpling and the potato starch. In the case of the potato starch, the fingers formed a pinch grasp such that the sensors on the inside of the fingertip had no contact with the object. For the yeast dumpling, the shear force sensors were in contact with the object but did slide along the surface without sticking, most likely due to its crumbly surface. The baseline approach did lift the dumpling but damaged it and failed to lift the jelly cup because the quickly moving index and thumb pushed the object out of the hand.

c) Damaged Objects: During the 31 grasp attempts executed for each approach, the baseline approach damaged nine objects (plastic and paper cup, both cans, boxed juice empty, toast, bananas, empty open PET bottle, paper-craft cube). The grasp-phases controller slightly pushed in the toast with the thumb, otherwise all objects where grasped and replaced without noticeable damage.

When placing objects, the grasp-phases controller managed to replace 22 objects in the same pose they were picked up, while the baseline managed to replace 23 objects correctly. The baseline used an accurate force-torque sensor while the grasp-phases controller relied on less accurate sensors of the finger tips. The primary failure of the controller was due to missing the placing event especially for soft objects, while the baseline toppled over tall objects or flung away light objects.

During our experiments the controller required on average $75\,\mu s$ on an *Intel(R) Core(TM) i7-6700 CPU @ 3.40GHz.*

V. Conclusion

We present a soft humanoid hand equipped with a multimodal sensor system in each finger to measure normal and shear forces, distance, joint configuration and tactile events. Further, we present a human-inspired grasp-phases controller that is able to detect different phases of a grasping an manipulation task and adapts object-hand interaction forces based on tactile feedback to allow safe grasping of completely unknown objects with different sizes, shapes and weight. This work extends existing human-inspired approaches to anthropomorphic hands and introduces an approach for synchronizing the actuators. We demonstrate the performance of the controller in experiments with 31 objects to evaluate the ability to balance forces at the contact points in precision and power grasps based on tactile feedback in the different phases of the task. The evaluation also demonstrates the ability of the grasp-phases controller to adapt forces while grasping fragile objects preventing their damage as well as to heavy objects. The implementation explicitly deals with incomplete sensor data while maintaining a low parameter count.

The experiments also revealed several shortcomings that will be addressed in our future work. In particular, the softness of the fingers makes slip detection challenging as the fingers slide uniformly over flat surfaces, making the detection of vibrations or sudden changes in shear force difficult. In the future we will conduct experiments with fingertip structures to induce noticeable vibrations during slip events. Slip detection would also allow a dynamic estimation of the currently constant friction coefficient. Further, grasping of thin and heavy box-shaped objects remains challenging as interaction with the objects is primary achieved through contacts with the very tip of the fingers. In our future work, we will work on further improvement of the finger tip sensor system in terms in miniaturization and signal robustness. This would also improve the controller behavior for the unload/placing phase, as this is currently solely dependent on the accelerometer signals. Detecting acceleration spikes is difficult when placing soft objects, as the impact will be dampened by the softness of the object.

REFERENCES

[1] A. Billard and D. Kragic, "Trends and challenges in robot manipulation," *Science*, vol. 364, no. 6446, 2019.

[2] Q. Li, O. Kroemer, Z. Su, F. F. Veiga, M. Kaboli, and H. J. Ritter, "A review of tactile information: Perception and action through touch," *Trans. on Robotics*, vol. 36, no. 6, pp. 1619–1634, 2020.

[3] H. Yussof, Masahiro Ohka, Hirofumi Suzuki, and Nobuyuki Morisawa, "Tactile sensing-based control algorithm for real-time grasp synthesis in object manipulation tasks of humanoid robot fingers," in *Int. Sym. on Robot and Human Interactive Communication*, 2008, pp. 377–382.

[4] N. Wettels, A. R. Parnandi, J.-H. Moon, G. E. Loeb, and G. S. Sukhatme, "Grip control using biomimetic tactile sensing systems," *Trans. On Mechatronics*, vol. 14, no. 6, pp. 718–723, 2009.

[5] T. Zhang, L. Jiang, X. Wu, W. Feng, D. Zhou, and H. Liu, "Fingertip three-axis tactile sensor for multifingered grasping," *Trans. on Mechatronics*, vol. 20, no. 4, pp. 1875–1885, 2015.

[6] M. R. Tremblay and M. R. Cutkosky, "Estimating friction using incipient slip sensing during a manipulation task," in *Int. Conf. on Robotics and Automation*, 1993, pp. 429–434 vol.1.

[7] A. Ajoudani, E. Hocaoglu, A. Altobelli, M. Rossi, E. Battaglia, N. Tsagarakis, and A. Bicchi, "Reflex control of the pisa/iit softhand during object slippage," in *Int. Conf. on Robotics and Automation*, 2016, pp. 1972–1979.

[8] M. Al-Mohammed, Z. Ding, P. Liu, and A. Behal, "An adaptive control based approach for gripping novel objects with minimal grasping force," in *Int. Conf. on Control and Automation*, 2018, pp. 1040–1045.

[9] K. Ganguly, B. Sadrfaridpour, K. B. Kidambi, C. Fermller, and Y. Aloimonos, "Grasping in the dark: Compliant grasping using shadow dexterous hand and biotac tactile sensor," 2020, uploaded to arxiv; arXiv:2011.00712.

[10] F. Veiga, B. Edin, and J. Peters, "Grip stabilization through independent finger tactile feedback control," *MDPI Sensors*, vol. 20, no. 6, 2020.

[11] A. Nakagawa-Silva, N. V. Thakor, J. Cabibihan, and A. B. Soares, "A bio-inspired slip detection and reflex-like suppression method for robotic manipulators," *IEEE Sensors*, vol. 19, no. 24, pp. 12 443–12 453, 2019.

[12] G. De Maria, P. Falco, C. Natale, and S. Pirozzi, "Integrated force/tactile sensing: The enabling technology for slipping detection and avoidance," in *Int. Conf. on Robotics and Automation*, 2015, pp. 3883–3889.

[13] Z. Su, K. Hausman, Y. Chebotar, A. Molchanov, G. E. Loeb, G. S. Sukhatme, and S. Schaal, "Force estimation and slip detection/classification for grip control using a biomimetic tactile sensor," in *Int. Conf. on Humanoid Robots*, 2015, pp. 297–303.

[14] M. Kaboli, K. Yao, and G. Cheng, "Tactile-based manipulation of deformable objects with dynamic center of mass," in *Int. Conf. on Humanoid Robots*, 2016, pp. 752–757.

[15] T. Takahashi, T. Tsuboi, KishidaTakeo, Y. Kawanami, S. Shimizu, M. Iribe, T. Fukushima, and F. Masahiro, "Adaptive grasping by multi fingered hand with tactile sensor based on robust force and position control," in *Int. Conf. on Robotics and Automation*, 2008, pp. 264–271.

[16] J. M. Romano, K. Hsiao, G. Niemeyer, S. Chitta, and K. J. Kuchenbecker, "Human-inspired robotic grasp control with tactile sensing," *Trans. on Robotics*, vol. 27, no. 6, pp. 1067–1079, 2011.

[17] H. Deng, G. Zhong, X. Li, and W. Nie, "Slippage and deformation preventive control of bionic prosthetic hands," *Trans. on Mechatronics*, vol. 22, no. 2, pp. 888–897, 2017.

[18] S.-Q. Ji, M.-B. Huang, and H.-P. Huang, "Robot intelligent grasp of unknown objects based on multi-sensor information," *MDPI Sensors*, vol. 19, no. 7, 2019.

[19] Z. Deng, Y. Jonetzko, L. Zhang, and J. Zhang, "Grasping force control of multi-fingered robotic hands through tactile sensing for object stabilization," *MDPI Sensors*, vol. 20, no. 4, 2020.

[20] A. Yamaguchi and C. G. Atkeson, "Implementing tactile behaviors using fingervision," in *Int. Conf. on Humanoid Robotics*, 2017, pp. 241–248.

[21] R. S. Johansson and J. R. Flanagan, "Coding and use of tactile signals from the fingertips in object manipulation tasks," *Nature Reviews Neuroscience*, vol. 10, no. 5, pp. 345–359, 2009.

[22] Y. She, C. Li, J. Cleary, and H.-J. Su, "Design and fabrication of a soft robotic hand with embedded actuators and sensors," *Journal of Mechanisms and Robotics*, vol. 7, no. 2, 2015.

[23] R. Deimel and O. Brock, "A novel type of compliant and underactuated robotic hand for dexterous grasping," *Int. Journal of Robotics Research*, vol. 35, no. 1-3, pp. 161–185, 2016.

[24] H. Zhao, K. OBrien, S. Li, and R. F. Shepherd, "Optoelectronically innervated soft prosthetic hand via stretchable optical waveguides," *Science robotics*, vol. 1, no. 1, 2016.

[25] J. Fras and K. Althoefer, "Soft biomimetic prosthetic hand: Design, manufacturing and preliminary examination," in *Int. Conf. on Intelligent Robots and Systems*, 2018, pp. 1–6.

[26] V. Wall and O. Brock, "Multi-task sensorization of soft actuators using prior knowledge," in *Int. Conf. on Robotics and Automation*, 2019, pp. 9416–9421.

[27] M. Ntagios, H. Nassar, A. Pullanchiyodan, W. T. Navaraj, and R. Dahiya, "Robotic hands with intrinsic tactile sensing via 3D printed soft pressure sensors," *Advanced Intelligent Systems*, vol. 2, no. 6, 2020.

[28] F. Hundhausen, J. Starke, and T. Asfour, "A soft humanoid hand with in-finger visual perception," in *Int. Conf. on Intelligent Robots and Systems*, 2020, pp. 8722–8728.

[29] P. Weiner, C. Neef, Y. Shibata, Y. Nakamura, and T. Asfour, "An embedded, multi-modal sensor system for scalable robotic and prosthetic hand fingers," *MDPI Sensors*, vol. 20, no. 1, pp. 108–121, 2019.

[30] N. Yamaguchi, S. Hasegawa, K. Okada, and M. Inaba, "A gripper for object search and grasp through proximity sensing," in *Int. Conf. on Intelligent Robots and Systems*, 2018, pp. 1–9.

[31] R. Koiva, T. Schwank, G. Walck, M. Meier, R. Haschke, and H. Ritter, "Barometer-based tactile skin for anthropomorphic robot hand," in *Int. Conf. on Intelligent Robots and Systems*, 2020, pp. 1–9.

[32] L. P. Jentoft, Q. Wan, and R. D. Howe, "Limits to compliance and the role of tactile sensing in grasping," in *Int. Conf. on Robotics and Automation*, 2014, pp. 6394–6399.

[33] T. Asfour, M. Wächter, L. Kaul, S. Rader, P. Weiner, S. Ottenhaus, R. Grimm, Y. Zhou, M. Grotz, and F. Paus, "Armar-6: A high-performance humanoid for human-robot collaboration in real world scenarios," *IEEE Robotics & Automation Magazine*, vol. 26, no. 4, pp. 108–121, 2019.